Biophysical Chemistry 140 (2009) 16–23

Contents lists available at ScienceDirect

Biophysical Chemistry

journal homepage: http://www.elsevier.com/locate/biophyschem

Poisson–Boltzmann model analysis of binding mRNA cap analogues to the translation initiation factor eIF4E

Oliwia Szklarczyk, Joanna Zuberek, Jan M. Antosiewicz *

Division of Biophysics, Institute of Experimental Physics, Department of Physics, University of Warsaw, Żwirki i Wigury 93, 02-089 Warszawa, Poland

ARTICLE INFO

Article history:
Received 17 September 2008
Received in revised form 7 November 2008
Accepted 7 November 2008
Available online 17 November 2008

Keywords:
Electrostatic binding energy
Dielectric boundary
Charge mutants

ABSTRACT

The electrostatic free energy of binding of two analogues of the 5′-mRNA cap, differing in size and electric charge, to the wild type and mutated eukaryotic initiation factor eIF4E was computed using the finite difference solutions to the Poisson–Boltzmann equation. Two definitions of the solute–solvent dielectric boundary were used: van der Waals model, solvent exclusion (SE) model. The computed electrostatic energies were supplemented by estimations of the non polar and entropic contributions. A comparison with experimental data for the investigated systems was done. It appears that the SE model with additional contribution fits experimental findings better than the van der Waals model does.

1. Introduction

Electrostatic interactions substantially contribute to the energetics of a variety of processes involving biomacromolecules [1]. One of the interesting aspects of electrostatic interactions is related to protein-ligand binding, where the term “ligand” refers to either a small molecule or another biomacromolecule. A high degree of complementarity of the charge distribution on the interfacing surfaces of associated molecules is frequently observed. One of the best known examples is the barnase–barstar complex [2,3]. Barnase is the extracellular ribonuclease produced by Bacillus amyloliquefaciens, and barstar is its intracellular inhibitor.

Because of the charge complementarity one may expect that electrostatic interactions favour formation of protein-ligand complexes. Such expectations were confirmed experimentally, among others, by an approach using site directed mutagenesis [4] to modify a charge at a particular site on the protein surface, originated by Fersht et al. [5]. For example, kinetic and equilibrium measurements with mutations of the residues in the barnase–barstar interface confirmed that neutralisation of charged residues within the interface significantly reduce the binding constant [6,7]. But in experiment, it is not possible to cleanly isolate electrostatic contributions from other factors. A physically sound approach to evaluate electrostatic energy is offered by a description of the solute–solvent system within the Poisson–Boltzmann (PB) model and a solution of the corresponding PB equation by the finite difference method (FDPB) [8]. The PB model treats the solute as a low-dielectric region bounded by the molecular surface and containing atomic charges at positions of the atomic nuclei determined e.g. by X-ray crystallography. When a given solute molecule possesses titratable groups, the partial charges assigned to atoms depend on the ionisation states of these groups. The solute is surrounded by a high-dielectric aqueous solvent which may contain a dissolved electrolyte. The mobile charge distribution in the solvent is described by the Boltzmann distribution, while electronic polarizability is implicitly included in the assumed dielectric constants of the media. The free energy of a given molecule, computed within the PB model, is given by the work required to assemble a set of n point charges, corresponding to the atomic partial charges, within the low-dielectric region [9]:

$$G_{\text{elec}} = \frac{1}{2}\sum_{k=1}^{n} q_k \phi_k \tag{1}$$

where ϕ_k is the electrostatic potential at the location of charge q_k. When the electrostatic potentials ϕ_k are computed as a solution to the appropriate Poisson–Boltzmann equation, with a requirement to satisfy boundary conditions imposed by the existence of the surfaces separating regions of different dielectric properties, they represent the total electrostatic potentials, considered to be the sum of the coulombic potentials due to all other charges except the charge k, plus the total reaction field at the location of the charge k, resulting from existence of the dielectric boundary. The electrostatic protein-ligand association energy is thus given by

$$\Delta G_{\text{elec}}^{\text{bind}} = \frac{1}{2}\sum_{k=1}^{n_{PL}} q_k^{(PL)}\phi_k^{(PL)} - \frac{1}{2}\sum_{k=1}^{n_P} q_k^{(P)}\phi_k^{(P)} - \frac{1}{2}\sum_{k=1}^{n_L} q_k^{(L)}\phi_k^{(L)} \tag{2}$$

where n_{PL}, n_P and n_L, are number of charges appropriate for the protein-ligand complex, the free protein and the free ligand, respectively. Eq. (2) describes the electrostatic effects on binding

* Corresponding author. Fax: +48 22 554 0771.
E-mail address: jantosi@biogeo.uw.edu.pl (J.M. Antosiewicz).

0301-4622/$ – see front matter © 2008 Elsevier B.V. All rights reserved.
doi:10.1016/j.bpc.2008.11.002

affinity, within approximation of a single (macro)molecular conformation fixed in a given protonation state.

PB calculations usually show that the electrostatic contribution to binding is unfavourable due to the large desolvation penalty of charged and polar groups which is not sufficiently compensated by the direct charge–charge interactions at the protein–ligand interface [1,10–13]. The unfavourable electrostatic contribution to the free energy of binding is usually obtained when the dielectric boundary is specified as the solvent exclusion (SE) surface along with solute dielectric constant in the range of about 2 to 4. Zhou and coworkers [14], studying the barnase and barstar complex, reduced the desolvation cost and the strength of charge–charge interactions by using the van der Waals (vdW) surface as the dielectric boundary and they obtained a negative electrostatic contribution of −11 kcal/mol to the binding free energy, for a protein dielectric constant (ε_P) of 4, and an ionic strength of 25 mM. However, the vdW surface of a protein molecule is surrounded by many small crevices, which are assigned the solvent (i.e. high) dielectric constant, therefore the physical correctness of this model might be not certain. Alexov [15] has noted the fact that X-ray crystallography does not identify many buried waters in proteins and therefore he considered vdW models to be not correct. But one might argue that the vdW model is consistent with ascribing protein interior slightly higher dielectric constant than that would result from only electronic polarizability, due to fluctuations in the conformation as a response to the electric field. The regions indicated as the crevices correspond to less densely packed regions of the protein, and one might expect even larger structural fluctuations in these regions than usually, what might be reflected by assigning still higher dielectric constant than just 4. Smoothing procedure used to ascribe dielectric constant to grid centres in the FDPB methods, results in the values of the dielectric constant between 4 and that ascribed to the solvent (i.e. about 80). Finally, we should also recall a work by Lee and Tidor [16] who have shown that by varying the atomic point charges of barstar they were able to make the electrostatic free energy of binding as low as −6.1 kcal/mol with the SE model for the dielectric boundary.

The vdW model of the solute–solvent dielectric boundary was shown by Zhou and coworkers [14] to exhibit one additional advantage over the SE model. They investigated electrostatic contributions to the binding stability of the 17 charge mutations neutralising charged residues lining the binding interface of barnase and barstar, and they concluded that the vdW model with ε_P=4 was most consistent with published experimental data, i.e. this model predicted an overall electrostatic stabilisation and quantitatively reproduced the observed effects of mutations. Similarly, in a case of protein–nucleic acid interactions, Qin and Zhou have found that the vdW model predicts stabilising electrostatic interactions for complex formation and also results in better agreement with experimental data regarding effects of charge mutations [17].

In this work, we compare SE and vdW models of the dielectric boundary referring to the system of eIF4E protein and analogs of 5′-end of mRNA. Association between eIF4E protein and 5′-end of mRNA is one of the essential steps in the initiation of eukaryotic mRNA translation [18]. The abbreviation “eIF4E” stands for a eukaryotic initiation factor 4E. Eukaryotic mRNAs possess a cap structure consisting of a 5′-5′-triphosphate bridge of a general form m^7GpppN, where m^7G is the 7-methylguanosine, and N can be any of the four nucleosides [19]. The crucial element of the cap recognition consists of sandwiching of the alkylated base between the side chains of two conserved tryptophans (Trp-56 and Trp-102 in the murine eIF4E). Moreover there is a number of hydrogen bonds stabilising the complex, N1 and N2 of m^7G make hydrogen bonds with the carboxylate oxygen atoms of Glu-103, and Arg-157 and Lys-162 make such contacts with oxygen atoms of the phosphate groups. Many of these hydrogen bonding interactions include contributions due to direct electrostatic interactions because the interacting groups are ionised. These insights into structural characteristics of cap-eIF4E complexes were mainly obtained from three-dimensional structures by X-ray crystallography [20–22] and multidimensional NMR study [23].

We computed electrostatic contributions to the binding free energy for three variants of eIF4E protein: wild type (wt), K159A mutant, and wt with phosphorylated Ser-209 (S209Sp), and two cap analogues: 7-methylguanosine 5′-triphosphate (m^7GTP), and 7-methylguanosine 5′-tetraphosphate (m^7Gp_4). The Ser-209 is phosphorylated in response to treatment of cells with growth factors, hormones and mitogens [18], and it was postulated that phosphorylation of Ser-209 could generate a salt bridge with Lys-159, which would introduce a retractable bridge covering the cap-binding slot near its entrance [20]. At the current state of crystallographic refinement, there is no well-localised electron density for the side chain of Lys-159 [20,21], therefore structural data for this chain must be obtained by molecular modelling methods. Employing the above variants of eIF4E protein and its ligands, we show that including reasonable evaluations of non polar and entropic contributions to the binding free energy, we obtain better agreement with the experimentally determined free energies of binding when SE model is used rather than the vdW model.

2. Materials and methods

2.1. Cap analogues, mutants of eIF4E, fluorescence titration measurements and experimental data

Synthesis of cap analogues, mutagenesis, expression and purification of eIF4Es, as well as fluorescence measurements and data analysis were described in detail elsewhere [24].

The binding of cap analogues to eIF4E can be followed by measurements of quenching of intrinsic tryptophan fluorescence of eIF4E, see e.g. [25], due to sandwich stacking between 7-methylguanine and two tryptophan indole rings [20,23]. The titration experiments were carried out in 50 mM Hepes/KOH (pH 7.2), 1 mM DTT, 0.5 mM EDTA and appropriate amount of KCl. Equilibrium association constants, K_{ass}, are determined by fitting the theoretical prediction for the fluorescence intensity on the total concentration of cap analogue to the measured titration data points.

Equilibrium binding constants, measured for investigated eIF4E-cap pairs, are presented in Table 1. They are calculated as an average of several independent titrations. The standard Gibbs free energy changes for complex formation were calculated from the K_{ass} values according to the standard equation $\Delta G^\circ = -RT\ln K_{ass}$. The presented equilibrium binding constants for complexes of wild type and mutated eIF4E protein with m^7GTP ligand were determined for the purpose of the present work, the remaining equilibrium binding constants connected to m^7Gp_4 ligand were reported previously [24].

Table 1
Equilibrium association constants, in units of [μM^{-1}], for the complexes of wild type and mutated eIF4E protein with m^7GTP and m^7Gp_4 analogues of 5′-mRNA terminus

KCl	ligand = m^7GTP			ligand = m^7Gp_4 [a]		
[mM]	wt	S209Sp	K159A	wt	S209Sp	K159A
50	–	107±6	114±7	–	385±23	337±24
100	145p±5	43.1±1.5	38.8±1.3	683±64	162±7	108±5
150	64.8±2.6	22.3±0.9	17.9±0.6	338±18	78.9±2.9	41.3±1.6
200	33.3±1.0	11.9±0.4	9.9±0.3	145±6	42.8±1.4	21.4±0.7
300	12.9±0.5	6.11±0.25	4.35±0.19	55.4±1.4	16.7±0.5	7.62±0.21
400	7.70±0.37	3.76±0.20	2.70±0.12	26.8±1.0	7.98±0.23	4.24±0.17
500	3.86±0.14	2.13±0.14	1.68±0.10	11.8±0.4	4.93±0.11	2.47±0.12

[a] Data taken from Ref. [24].

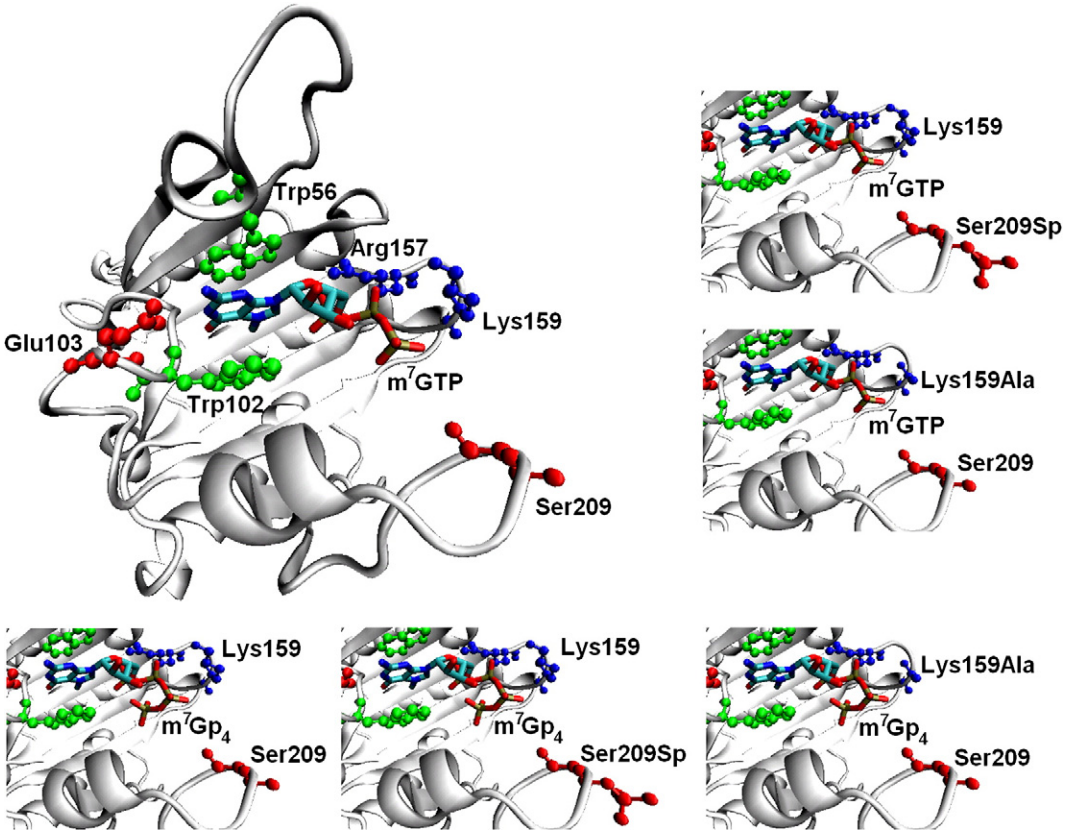

Fig. 1. Structure of the original eIF4E:m^{7}GTP complex and structures of the vicinity of the binding site for different variants of the protein and ligand.

2.2. Computational procedures

For our calculations we used a crystal structure of truncated murine eIF4E (28–217) complexed with a dinucleotide cap analogue, m^{7}GpppG, available from the Protein Data Bank (PDB) [26], under accession code 1L8B [21]. Monomer B of this structure was used.

The PDB file does not contain coordinates for the second guanosine of the dinucleotide cap analogue, which is missing in the electron density because of high flexibility. Therefore, the coordinates present in the original structural file can be used as representing just the complex of eIF4E with m^{7}GTP. Missing heavy atoms, e.g. those corresponding to the side chain of Lys-159 in eIF4E protein, discussed above, were built in with the molecular dynamics program CHARMM [27]. Hydrogen atoms were added to the structures using the CHARMM routine HBUILD. The protein mutants K159A and S209Sp, as well as cap analogue m^{7}Gp$_4$ were modelled using also CHARMM. The model-built fragments were energy minimised using CHARMM, and the CHARMM27 parameters, and force field [28,29]. In all minimisations we used 1000 steps of the Steepest Descents followed by 1000 steps of Adopted Basis Newton–Raphson minimisation algorithms, implemented in CHARMM.

For the purpose of relaxing added heavy atoms missing in the original PDB file, or model-built mutants, we added hydrogen atoms at the amount corresponding to protonation states of titratable residues expected for neutral pH, and then the coordinates of the added atoms were energy-minimised using CHARMM, while all heavy atoms present in the original PDB file were kept fixed. Then hydrogen coordinates were stripped from the data sets, and the resulting structures were treated as starting structures for the six complexes of the eIF4E protein (wt, S209Sp, K159A) and the cap analogues (m^{7}GTP, m^{7}Gp$_4$). These structures are shown in Fig. 1. The central part presents eIF4E-wt protein complexed with m^{7}GTP. Neighbouring panels illustrate structures with mutated amino acids and/or mutated ligand. The protein is shown in a ribbons representation. Important protein's residues are shown in the ball-and-stick representation: Trp-56 and Trp-102, important for the ligand binding and directly involved in the fluorescence quenching experiments, are shown in green, the Glu-103 and Ser-209 are red, Arg-157, Lys-159 and Lys-162 are blue. The ligands are shown in stick representation, with the sticks coloured according to the chemical elements (colors are visible only in the on-line version of the paper).

Analysis of electrostatic contributions to protein-ligand association energy requires that protonation states of their ionizable groups for given solution conditions are determined. The protonation probabilities of titratable groups in the eIF4E protein and terminal phosphate groups of m^{7}GTP, m^{7}Gp$_4$ ligands, corresponding to experimental conditions of the fluorescence titration measurements [24], were calculated as described in detail elsewhere [30,31], using the University of Houston Brownian Dynamics program (UHBD) [32,33]. For the purpose of predicting titration equilibria, all hydrogens were added and optimised with respect to their positions using CHARMM. During this hydrogens optimisation, non hydrogen atoms were kept fixed. The titration curves were computed using a Monte Carlo (MC) approach described elsewhere [34]. The MC program provides a list of a predefined number of the protonation states of the investigated molecules with the lowest free energies found during the MC search. The calculations were done for the apo-form of eIF4E protein, and for eIF4E complexes with the two cap analogues. Besides standard titratable groups in proteins, also the terminal phosphate group of the ligands and the phosphate group of the Ser 209 (for their secondary titration) were treated as ionizable. All predicted protonation states refer to pH of 7.2, the same as that used in the experiments [24].

The electrostatic potentials for the protein-ligand and isolated protein or isolated ligand were calculated using the FDPB method implemented in the UHBD program. The linearised Poisson–Boltzmann equation was used in these calculations. Subsequently, the electrostatic

energies of the molecules were computed according to Eq. (1). To minimise numerical errors, the protein and ligand were in the same conformation and were placed in the same position in the grid both in the isolated and complexed states. Note that when the difference in Eq. (2) is taken with the charges located in the same position on the finite difference grid in all calculations of the electrostatic potential, the arbitrary coulombic self-energy terms cancel.

All simulations were performed at 293 K (RT=0.58 kcal/mol), at ionic strengths corresponding to 50, 100, 150, 200, 300, 400 and 500 mM added KCl, with a solvent dielectric constant of 80, and that for the protein 4. The protein and cap analogues interiors were defined either by Richards probe-accessible surface [35], computed with a probe of radius 1.4 Å, and an initial dot density of 500 per atom [36] (nmap 1.4, nsph 500) or as the regions within the van der Waals surface, selected by turning off the "nmap 1.4, nsph 500" option. Dielectric boundary smoothing [37] was used in all finite difference calculations.

We made use of finite difference "focusing" [38] in order to improve accuracy of our electrostatic calculations. The first grid always encompassed the entire molecule(s) plus an adequate solvent region (135^3 cubic grid with a 2.7 Å spacing). For prediction of titration equilibria, subsequently three finer grids, centred at the current titratable group were used: 60^3, 1.4 Å; 50^3, 0.7 Å; 45^3, 0.5 Å, respectively. For electrostatic binding free energy calculations two finer grids were used: 135^3, 1.4 Å; 135^3, 0.5 Å, respectively. The smallest grid for electrostatic binding energy calculations also encompassed the entire molecule(s).

2.3. Other than electrostatic contributions to the free energy

Additional contributions to the binding free energy were estimated using a method described elsewhere [10]. The equation for ΔG^{bind} used in this report is as follows:

$$\Delta G^{\text{bind}} = \Delta G^{\text{es}} + \Delta G^{\text{np}} + \Delta G^{\text{strain}} - T\Delta S^{\text{conf}} - T\Delta S^{t,r} \quad (3)$$

The above formula assumes that there is no correlation between the components. This is a useful method to study the influence of certain changes in the system (e.g. mutations) on the thermodynamic stability and processes that the system undergoes. Eq. (3) consists of the electrostatic term (ΔG^{es}), the non polar term (ΔG^{np}), the term corresponding to small conformational changes in the system caused by the tension occurring during the process (ΔG^{strain}), the term describing loss of the conformational degrees of freedom ($-T\Delta S^{\text{conf}}$), and finally the term corresponding to the loss of the rotational and translational degrees of freedom ($-T\Delta S^{t,r}$).

Calculation of the first component has been described above. The non polar contribution was estimated applying a model of the solvent accessible surface area (SASA) [39], in which the change of the free energy corresponding to non polar interactions is proportional to the change of SASA:

$$\Delta G^{\text{np}} = \Gamma_{aw}\Delta SASA + b \quad (4)$$

$$\Delta SASA = SASA_{PL} - (SASA_p + SASA_L) \quad (5)$$

where Γ_{aw} is the microscopic surface tension coefficient and b is the coefficient of the linear fit to experimental data concerning transfer of short alkanes from aqueous alkanes to water. We used values of these coefficients typical for a protein-RNA complex, Γ_{aw}=0.005 kcal/mol/Å and b=0.92 kcal/mol [40]. The non polar component is an energy change of reorganisation of the solvent molecules due to a reduction of the molecule surface accessible for the solvent. In the association process it gives always a negative contribution.

Atoms at the surface of the molecules involved in binding have usually less degrees of conformational freedom than in the unbound form of the molecules [41]. The $-T\Delta S^{\text{conf}}$ term in Eq. (3) is a sum of a component responsible for the loss of the main chain ($-T\Delta S^{\text{conf}}_{mc}$) and the side chain ($-T\Delta S^{\text{conf}}_{sc}$) atoms' conformational degrees of freedom:

$$-T\Delta S^{\text{conf}} = -T\Delta S^{\text{conf}}_{mc} - T\Delta S^{\text{conf}}_{sc} \quad (6)$$

Estimated experimental values of the main chain contribution to the binding free energy, in temperature of about 300K, range from 0.5 to 2 kcal/mol per each carbon–carbon single bond fixed to a single rotamer [42]. Theoretical works assess this contribution to be between 0.3 and 0.48 kcal/mol [43](and references therein). In this study we use the value 0.54 kcal/mol suggested by the empirical Pickett and Sternberg scale [44]. The side chain term in Eq. (6) was estimated following [10], where an average value of 2 kcal/mol had been ascribed to every residue buried in the interface between the interacting molecules.

The two remaining components present in Eq. (3), ΔG^{strain} and $-T\Delta S^{t,r}$, give positive contributions to the total free energy of association. The upper limit for ΔG^{strain} is 10 kcal/mol, which is the free energy of folding of a typical protein [10]. To calculate the $-T\Delta S^{t,r}$, the range of residual motion in the complex must be known. Based on atomic motions in crystals, Finkelstein and Janin [42] estimate an entropy loss of 50 cal/mol K, what leads for temperature of 293 K to about 15 kcal/mol. Other authors noticed that amplitudes of motions in the complex in solution are larger than those found in the crystal, hence the estimations of the $-T\Delta S^{t,r}$ are correspondingly smaller. Minh and coworkers estimated the entropic cost of acetylcholinesterase binding to fasciculin-2 as 30 cal/mol K [45], what leads to about 9 kcal/mol at room temperature. Luo and Gilson [47] for the binding of adenine to synthetic adenine receptors and Hermans and Wang [46] for the binding of benzene to a lysozyme cavity, obtained $-T\Delta S^{t,r}$ of about 7 kcal/mol. Lazaridis and coworkers based on molecular dynamics simulations with implicit solvation of the binding of biotin, biotin analogs and two peptides to avidin and streptavidin [43], estimated $-T\Delta S^{t,r}$ as about 6 kcal/mol. Taking all these estimates into account, we assume in the present work that the components ΔG^{strain} and $-T\Delta S^{t,r}$ contribute jointly +15 kcal/mol.

3. Results and discussion

3.1. Predicted protonation states and other structural aspects

We begin with the terminal phosphate groups of m^7GTP and m^7Gp_4. The predicted ionisation constant for the secondary titration of these phosphate groups depends on the choice of the protonation site in the group, i.e. which of the three oxygen atoms, O1G, O2G and O3G in m^7GTP (names according to the PDB files nomenclature) and O1D, O2D and O3D in m^7Gp_4 (names introduced in this work analogously to the case of m^7GTP) binds the proton. This is because we perform our calculations for rigid structures. Table 2 shows pK_a values for each of these oxygens in both ligands obtained for ionic strength of 150 mM. For m^7GTP all three values are similar. On the contrary, for the m^7Gp_4 ligand the hydrogen atom is most stable when bound to the O3D oxygen. In both cases we decided to choose the O3 oxygen as the protonation place.

Table 2
Protonation states of the ligand — pKa values for each of the oxygen of the terminal phosphate groups for ionic strength of 150 mM

Protonation site	pK_a
M^7GTP-O1G	7.46
m^7GTP-O2G	6.90
m^7GTP-O3G	7.48
m^7Gp_4-O1D	11.59
m^7Gp_4-O2D	11.79
m^7Gp_4-O3D	14.85

Table 3
Protonation states of selected residues in the six lowest energy states obtained from Monte Carlo calculations for indicated forms of eIF4E-cap complex, at ionic strength of 150 mM

Complex	Q	Residues						
		His-37	Glu-103	Arg-157	Lys-159	Lys-162	Ser-209	M^7GTP
Wt-m^7GTP	+2	101011	000000	111111	000000	111111		001100
S209Sp-m^7GTP	+2	101010	000000	111111	000000	111111	111100	001100
K159A-m^7GTP	+2	101011	000000	111111		111111		001100
Wt-m^7Gp_4	+2	101100	000000	111111	000000	111111		111111
S209Sp-m^7Gp_4	+2	101011	000000	111111	000000	111111	110011	111111
K159A-m^7Gp_4	+2	101100	000000	111111		111111		111111

Subsequently, protonation probabilities of all combinations of the complex in ionic strengths 50, 100, 150, 200, 300, 400 and 500 mM were calculated. An example of the predicted protonation states of selected residues in the most stable state are shown in Table 3). In all cases the most probable ionizable state (the one with the lowest energy) for the ligand m^7GTP was an ionised O3G oxygen, while for the m^7Gp_4 ligand the O3D oxygen was protonated. The complexed protein (with either m^7GTP or m^7Gp_4) shows identical protonation patterns in the lowest energy state in the ionic strength range of 50–300 mM. The states change when a higher ionic strength is applied. This is because one of the five histidines present in eIF4E, His37, changes from a protonated to a deprotonated form when the ionic strength is increased to 400 mM, thus the total charge of the complex diminishes with −1. In the wt and S209Sp complexes the amino acid Lys-159 remains in a deprotonated form in all six lowest energy states.

For each case, i.e. apo-eIF4E and its complex with cap analogues, the predicted protonation states of protein's titratable sites surrounding the binding site, for several lowest energy states are the same. These lowest energy states differ only in protonation states of some distant titratable groups. Therefore electrostatic binding energies reported here were computed for the most stable protonation state.

One interesting result of these computer titrations refers to predicted deprotonated state of Lys-159. Along the protein chain, this residue is close to two other basic amino acids: Arg-157 and Lys-162. The latter are firmly protonated at pH of 7.2, both in the apo-protein and in the complexes with cap analogues. The interaction between the negatively charged phosphate groups and Arg-157 and Lys-162 shifts pK_a values for these amino acids by at least several pH units up. Neutrality of Lys-159 at pH about 7 does not result from electrostatic interactions with Arg-157 and Lys-162. Neutralisation of the latter residues only slightly increases pK_a of Lys-159, and it remains firmly neutral at pH of 7.2. Neither association with cap influences pK_a of Lys-159 to make it charged at that pH. This is an interesting result in light of hypothesis regarding possible salt bridge between Lys-159 and phosphorylated Ser-209 [20]. According to our calculation phosphorylated Ser-209 does not undergo secondary ionisation at neutral pH, neither in the complex with m^7GTP nor with m^7Gp_4 (see Table 3). Therefore results of our calculation contradict existence of such a salt bridge.

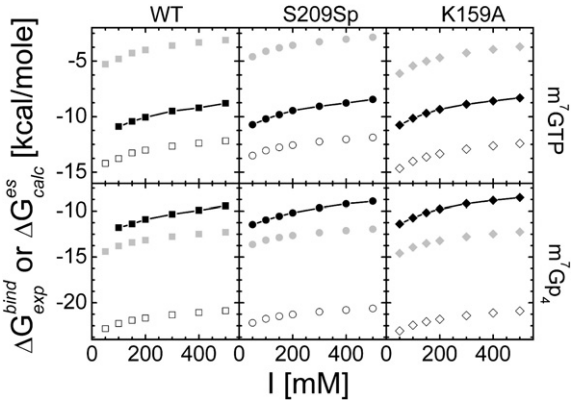

Fig. 2. Comparison of ionic strength dependence of experimentally determined free energies of binding (black symbols joined by lines) with computed electrostatic contributions. Empty and grey filled symbols refer to vdW and SE dielectric boundary models, respectively.

3.2. Computed electrostatic contributions

Computed changes of the electrostatic free energy upon complex formation, in both SE and vdW models, give negative contributions to the total free energy of binding (see Table 4). Thus both models predict a stabilising effect of the electrostatic interactions during the binding process. In Fig. 2, the computed electrostatic contributions to the free energy of binding for all protein and ligand variants and all ionic strengths are compared with the free energies of binding obtained from experiments.

For the m^7GTP ligand the vdW model predicts values of ΔG^{es} that are lower than the experimental ΔG^{bind} values of about 5 kcal/mol, which is equivalent to an underrating of the experimental value. The SE model overrates the experimental values about 6 kcal/mol, although it also predicts a stabilising electrostatic effect. As for the

Table 4
Calculated electrostatic free energies (in units of kcal/mol) for different variants of eIF4E-cap complexes, and ionic strengths

KCl [mM]	m^7GTP	model = SE			model = vdW		
		wt	S209Sp	K159A	wt	S209Sp	K159A
50		−5.29	−4.61	−6.11	−14.2	−13.5	−14.7
100		−4.81	−4.12	−5.43	−13.8	−13.1	−14.0
150		−4.28	−3.81	−5.01	−13.3	−12.8	−13.6
200		−4.01	−3.58	−4.70	−13.0	−12.6	−13.3
300		−3.61	−3.27	−4.26	−12.7	−12.3	−12.9
400		−3.33	−3.03	−3.95	−12.4	−12.0	−12.6
500		−3.12	−2.85	−3.71	−12.2	−11.9	−12.4
	m^7Gp_4						
50		−14.4	−13.6	−14.6	−22.8	−22.2	−23.1
100		−13.8	−13.2	−13.9	−22.3	−21.7	−22.5
150		−13.4	−12.9	−13.5	−21.9	−21.5	−22.1
200		−13.2	−12.7	−13.2	−21.7	−21.3	−21.8
300		−12.8	−12.4	−12.8	−21.3	−21.0	−21.4
400		−12.5	−12.1	−12.5	−21.1	−20.8	−21.1
500		−12.3	−12.0	−12.3	−20.9	−20.6	−20.9

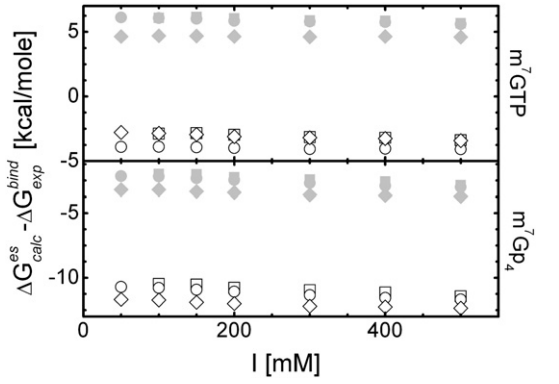

Fig. 3. Differences between computed electrostatic free energies of binding and experimentally determined free energies of binding as functions of the ionic strength. Open and grey filled symbols refer to vdW and SE dielectric boundary models, respectively. Wild type of eIF4E — circles; K159A mutant — squares; S209Sp mutant — diamonds.

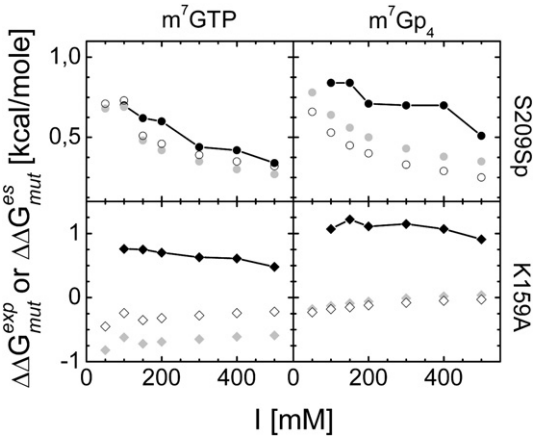

Fig. 4. Effects of protein mutations shown as $\Delta\Delta G^{es}=\Delta G^{es}_{mut}-\Delta G^{es}_{wt}$, for computed electrostatic binding free energies (grey and empty symbols). For a comparison analogous results obtained from experimentally determined binding free energies are also shown (black symbols connected by lines).

ligand with an additional phosphate group, both models underrate the ΔG^{bind} value, SE predicts 2–4 kcal/mol lower values, while the vdW model — 11–12 kcal/mol lower values. Results of the calculations provided for all types of combinations show that the ligands bind most strongly to the K159A form of the enzyme. This is inconsistent with the experiments which indicate the wt form to bind most strongly.

3.3. Salt effects

It can be seen also in Fig. 2 that the computed electrostatic contributions and the experimental binding free energies have very similar ionic strength dependencies. This is further confirmed by Fig. 3 showing differences between the computer electrostatic contributions and the experimental binding free energies for changing ionic strength. All differences are almost ionic strength independent. The slopes of the linear relations shown in Fig. 3 are between 0.0002 and 0.002 kcal/mM, thus very close to 0.

3.4. Energetic effects of mutations

We can also look at our data from perspective of energetic effects of mutations. The effects of mutations in the eIF4E protein, i.e. the differences $\Delta\Delta G^{es}_{mut}=\Delta G^{es}_{mut}-\Delta G^{es}_{wt}$ are shown in Fig. 4. Subsequently, Fig. 5 shows effects of mutation in the ligand (i.e. addition of the fourth phosphate group to m7GTP is considered as a mutation in the ligand), $\Delta\Delta G^{es}_{mut}=\Delta G^{es}_{m^7Gp_4}-\Delta G^{es}_{m^7GTP}$. For comparison, analogous differences obtained using experimentally determined binding energies are shown in both Figures. Taking into account a degree of the agreement between computed and experimental $\Delta\Delta G_{mut}$ we should conclude that neither of the two models of the dielectric boundary is better than the other.

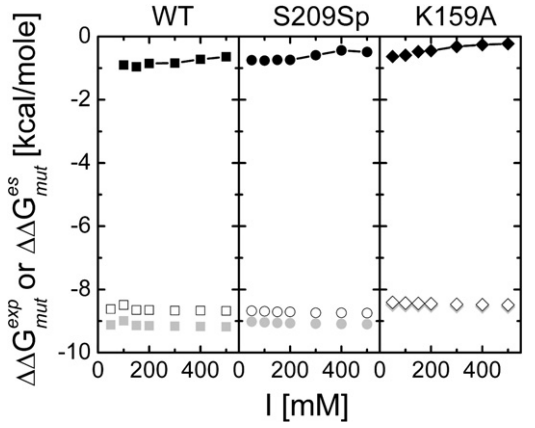

Fig. 5. Effects of ligand mutations shown as $\Delta\Delta G^{es}=\Delta G^{es}_{Gp_4}-\Delta G^{es}_{GTP}$, for computed electrostatic binding free energies (grey and empty symbols are for SE and vdW models, respectively). For a comparison analogous results obtained from experimentally determined binding free energies are also shown (black symbols connected by lines).

Table 5
Additional estimated components to the binding free energy, in units of [kcal/mol]

	wt		S209Sp		K159A	
	ΔG^{np}	$-T\Delta S^{conf}$	ΔG^{np}	$-T\Delta S^{conf}$	ΔG^{np}	$-T\Delta S^{conf}$
M^7GTP	−43.3	16.5	−42.3	16.5	−42.3	15.9
M^7Gp_4	−46.3	19.2	−46.2	20.3	−46.2	19.2

When the protein mutation is considered, we can see in Fig. 4 that the results obtained for the S209Sp mutation and the m^7GTP ligand are almost quantitatively consistent with the experimental results. Mutation K159A leads to a worse agreement with the experiment, probably because this mutation requires more advanced modelling of structural changes in the protein upon the mutation than those employed in our study. Also the worse agreement with the experiment obtained for m^7Gp_4 cap analogue and S209Sp mutation is most probably caused by not fully adequate modelling of the mutated ligand structure. When the ligand mutation is considered, we can see in Fig. 5 that for all three forms of the protein the deviations between computation and experiment are much larger than in the case of the protein mutations. All these most probably points to the necessity of more advanced modelling mutated structures. But most important from the perspective of the present investigation is that effects of charge mutations do not differentiate the two calculation protocols as obtained by Zhou and coworkers, who applied similar way of modelling mutated structures as those employed here.

3.5. Estimation of the remaining contributions

Table 5 presents non polar and conformation related entropic contributions to the binding free energies for systems investigated in this work, evaluated as described above. The non polar term in Eq. (3) gives a large negative contribution to the binding free energy for all complexes (42–47 kcal/mol). Theoretical binding energies including all terms are called ΔG^{bind}. The entropic terms give a positive contribution of about 16–20 kcal/mol. The remaining terms ΔG^{strain}) and $-T\Delta S^{t,y}$ raise ΔG^{bind} with +15 kcal/mol, as was described above.

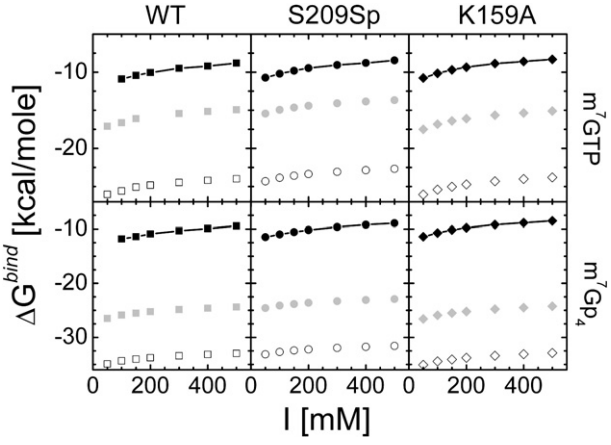

Fig. 6. Comparison of ionic strength dependence of experimentally determined free energies of binding (black symbols joined by line) with total computed binding energies. Empty and grey filled symbols refer to vdW and SE dielectric boundary models, respectively.

3.6. Effects of including the additional contributions

We compare ΔG^{bind} described in the previous section with experimental binding energies in Fig. 6. After taking into account the additional contributions to the ΔG^{bind} one can still observe the same ionic strength dependency conserved, just as in Fig. 2. The values predicted by the SE model are still higher than those obtained from the vdW model, nevertheless the former does not overrate the experimental values anymore. Both models underrate the experimental values. For the m^7GTP complexes the SE model predicts values about 6–7 kcal/mol lower, and the vdW model predicts values about 15–16 kcal/mol lower. As for the m^7Gp_4 complexes we obtained results underrating the experimental ones with about 15 kcal/mol within the SE model and about 23–24 kcal/mol within the vdW model. It should be noted that for the additional contributions we took some average estimates, therefore it can be expected that positive contributions are underestimated. However, for the vdW model these positive contributions must by about 10 kcal/mol larger than those for the SE model required to obtain agreement with the experimental data. Therefore we consider that the results presented in Fig. 6 indicate that the SE model is more appropriate.

4. Conclusions

If one compares the results of computed electrostatic binding free energy with the experimental data, the vdW model might show better agreement with experiment in comparison to the SE model, as was obtained by Zhou and coworkers [14,17]. Their conclusion was based on two findings: the vdW model predicted electrostatic stabilisation of the complexes, and this model agreed better with effects of charge mutations in the associating proteins. In the case of eIF4E-cap complexes, investigated in the present study, both models predict a stabilising effect of the electrostatic forces on binding, with the vdW model giving more negative binding energies by 8–9 kcal/mol than those predicted by the SE model. Both models predict similar salt effects of the electrostatic contribution, as well as influence of the mutations. Therefore, we found that neither SE nor vdW model shows substantially better agreement with the experimental data in comparison to the other model. A further analysis, including non-electrostatic contributions to binding energy, appeared essential in order to discriminate between the two Poisson–Boltzmann models. We showed that including the entropic, non polar and other important terms to the free energy function predicts a better agreement of the SE model than the vdW model with experimental data. Here, only a rough estimation of non-electrostatic contributions was performed in order to show the effects of these additional contributions to the binding free energy that were not taken into account by Zhou and coworkers [14,17]. It should be noted that the uncertainty in the estimated non-electrostatic terms may be quite substantial, although it is difficult to provide their accurate estimate. For computation of non-electrostatic terms we adapted methods described by Honig et al. [39,10] and by Beveridge et al. [40]. Both groups have found that the estimated total free energies of binding were overestimated. This overestimation would be greater with the vdW model for the dielectric boundary, what supports conclusions of the present work. However we should add that some consistent coupling of non polar and polar solvation free energies in the context of computation of the binding free energies is desired and such work is in progress [48]. It is also useful to point to recent important improvements in modelling non polar contributions to free energy of binding, particularly a recognition of non polar attractive and repulsive contributions to free energy of binding which must be modelled separately [49–51].

Beveridge and coworkers also pointed to the necessity of careful simulation of conformational adaptation following mutations [40]. In the present work and in the work of Zhou and coworkers relatively simple approach with respect to this problem was used. Zhou and coworkers modelled mutations in Insight II, followed by energy minimisation. In the present work mutants were modelled using CHARMM and energy minimisation. Better agreement of charge mutations obtained by Zhou for vdW model might result from cancellation of some opposite effects. It is rather clear that for more realistic results molecular dynamics simulations of mutants with explicit solvent are necessary. One can add that because there are some ionizable groups present at the interface between the associating molecules, such simulations should also consider possible changes in protonational preferences of these groups upon binding. Recent investigation by our group with respect to protein–protein binding provides some evidences for importance of this factor [52]. Because all these improvements make a computationally demanding project by itself, such analysis will be a subject of another study.

Acknowledgement

This study was supported by National Science Support Project 2008-2010 (JZ, No. PBZ-MNiSW-07/I/2007), and by University of Warsaw (JMA, BST-1239/BF).

References

[1] B. Honig, A. Nicholls, Classical electrostatics in biology and chemistry, Science 268 (1995) 1144–1149.
[2] A.M. Buckle, G. Schreiber, A.R. Fersht, Protein–protein recognition: Crystal structural analysis of a barnase–barstar complex at 2.0 Å resolution, Biochemistry 33 (1994) 8878–8889.
[3] L.P. Lee, B. Tidor, Barstar is electrostatically optimized for tight binding to barnase, Nature Struct. Biol. 8 (2001) 73–76.
[4] C.A. Hutchison III, S. Phillips, M.H. Edgell, S. Gillam, P. Jahnke, M. Smuith, Mutagenesis at a specific position in a DNA sequence, J. Biol. Chem. 253 (1978) 6551–6560.
[5] P.G. Thomas, A.J. Russell, A.R. Fersht, Tailoring the pH dependence of enzyme catalysis using protein engineering, Nature 318 (1985) 375–376.
[6] G. Schreiber, A.R. Fersht, Energetics of protein–protein interactions: Analysis of the barnase–barstar interface by single mutations and double mutant cycles, J. Mol. Biol. 248 (1995) 478–486.
[7] C. Frisch, G. Schreiber, C.J. Johnson, A.R. Fersht, Thermodynamics of the interaction of barnase and barstar: Changes in free energy versus changes in enthalpy on mutation, J. Mol. Biol. 267 (1997) 696–706.
[8] J. Warwicker, H.C. Watson, Calculation of the electric potential in the active site cleft due to α-helix dipoles, J. Mol. Biol. 157 (1982) 671–679.
[9] C.J.F. Böttcher, Theory of electric polarization, vol. I, Elsevier, Amsterdam, 1973.
[10] N. Froloff, A. Windemuth, B. Honig, On the calculation of binding free energies using continuum methods: Application to MHC class I protein–peptide interactions, Prot. Sci. 6 (1997) 1293–1301.
[11] T. Lazaridis, Binding affinity and specificity from computational studies, Cur. Org. Chem. 6 (2002) 1319–1332.
[12] J.M.J. Swanson, R.H. Henchman, J.A. McCammon, Revisiting free energy calculations: A theoretical connection to MM/PBSA and direct calculation of the association free energy, Biophys. J. 86 (2004) 67–74.
[13] K. Brock, K. Talley, K. Coley, P. Kundrotas, E. Alexov, Optimization of electrostatic interactions in protein–protein complexes, Biophys. J. 93 (2007) 3340–3352.
[14] F. Dong, M. Vijayakumar, H.X. Zhou, Comparison of calculation and experiments implicates significant electrostatic contributions to the binding stability of barnase and barstar, Biophys. J. 85 (2003) 49–60.
[15] E. Alexov, Role of the protein side-chain fluctuations on the strength of pair-wise electrostatic interactions: comparing experimental with computed pK_αs, Proteins 50 (2003) 94–103.
[16] L.P. Lee, B. Tidor, Optimization of binding electrostatics: Charge complementarity in the barnase–barstar protein complex, Prot. Sci. 10 (2001) 362–377.
[17] S. Qin, H.X. Zhou, Do electrostatic interactions destabilize protein-nucleic acid binding? Biopolymers 86 (2007) 112–118.
[18] N. Sonenberg, mRNA 5′ cap-binding protein eIF4E and control of cell growth, in: J. Hershey, M.B. Mathews, N. Sonenberg (Eds.), Translation Control, Cold Spring Harbor Laboratory Press, New York, 1996, pp. 245–269.
[19] A.J. Shatkin, Capping of eukaryotic mRNAs, Cell 9 (1976) 645–653.
[20] J. Marcotrigiano, A. Gingras, N. Sonenberg, S.K. Burley, Cocrystal structure of the messenger RNA 5′ cap-binding protein (eIF4E) bound to 7-methyl-GDP, Cell 89 (1997) 951–961.
[21] A. Niedźwiecka, J. Marcotrigiano, J. Stępiński, M. Jankowska-Anyszka, A. Wysłouch-Cieszyńska, M. Dadlez, A. Gingras, P. Mak, E. Darżynkiewicz, N. Sonenberg, S.K. Burley, R. Stolarski, Biophysical studies of eIF4E cap-binding protein: Recognition mRNA 5′ cap structure and synthetic fragments of eIF4G and 4E-BP1 proteins, J. Mol. Biol. 319 (2002) 615–635.
[22] K. Tomoo, X. Shen, K. Okabe, Y. Nozoe, S. Fukuhara, S. Morino, M. Sasahi, T. Taniguchi, H. Miygawa, K. Kitamura, K. Miura, T. Ishida, Structural features of

human initiation factor 4E studied by X-ray crystal analysis and molecular dynamics simulations, J. Mol. Biol. 328 (2003) 365–383.
[23] H. Matsuo, H. Li, A.M. McGuire, C.M. Fletcher, A. Gingras, N. Sonenberg, G. Wagner, Structure of translation factor eIF4E bound to m7GDP and interaction with 4E-binding protein, Nature Struct. Biol. 4 (1997) 717–724.
[24] J. Żuberek, J. Jemielity, A. Jabłonowska, J. Steępiński, M. Dadlez, R. Stolarski, E. Darżynkiewicz, Influence of electric charge variation at residues 209 and 159 on the interaction of eIF4E with the mRNA 5′ terminus, Biochemistry 43 (2004) 5370–5379.
[25] S.E. Carberry, R.E. Rhoads, D.J. Goss, A spectroscopic study of binding of m7GTP and m7GpppG to human protein synthesis initiation factor 4E, Biochemistry 28 (1989) 8078–8082.
[26] F.C. Bernstein, T.F. Koettzle, G.J.B. Williams, E.F. Meyer, M.D. Brice, J.R. Rodgers, O. Kennard, T. Shimanouchi, M.J. Tasumi, The protein data bank: a computer-based archival file for molecular structures, J. Mol. Biol. 123 (1977) 557–594.
[27] B.R. Brooks, R.E. Bruccoleri, B.D. Olafson, D.J. States, S. Swaminathan, M. Karplus, CHARMM: A program for macromolecular energy, minimization, and dynamics calculations, J. Comput. Chem. 4 (1983) 187–217.
[28] A.D. MacKerell Jr., D. Bashford, M. Bellott, R.L. Dunbrack Jr., J.D. Evanseck, M.J. Field, S. Fischer, J. Gao, H. Guo, S. Ha, D. Joseph-McCarthy, L. Kuchnir, K. Kuczera, F.T.K. Lau, C. Mattos, S. Michnick, T. Ngo, D.T. Nguyen, B. Prodhom, W.E. Reiher III, B. Roux, M. Schlenkrich, J.C. Smith, R. Stote, J. Straub, M. Watanabe, J. Wiorkiewicz-Kuczera, D. Yin, M. Karplus, All-atom empirical potential for molecular modeling and dynamics studies of proteins, J. Phys. Chem. B 102 (1998) 3586–3616.
[29] N. Foloppe, A.D. MacKerell Jr., All-atom empirical force field for nucleic acids: I. Parameter optimization based on small molecule and condensed phase macromolecular target data, J. Comp. Chem. 21 (2000) 86–104.
[30] J. Antosiewicz, J.M. Briggs, A.E. Elcock, M.K. Gilson, J.A. McCammon, Computing the ionization states of proteins with a detailed charge model, J. Comp. Chem. 17 (1996) 1633–1644.
[31] J.M. Briggs, J. Antosiewicz, Simulation of pH-dependent properties of proteins using mesoscopic models, Rev. Comput. Chem. 13 (1999) 249–311.
[32] M.E. Davis, J.D. Madura, B.A. Luty, J.A. McCammon, Electrostatics and diffusion of molecules in solution: Simulations with the University of Houston Brownian Dynamics program, Comp. Phys. Commun. 62 (1991) 187–197.
[33] J.D. Madura, J.M. Briggs, R.C. Wade, M.E. Davis, B.A. Luty, A. Ilin, J. Antosiewicz, M.K. Gilson, B. Bagheri, L.R. Scott, J.A. McCammon, Electrostatics and diffusion of molecules in solution: Simulations with the University of Houston Brownian Dynamics program, Comput. Phys. Commun. 91 (1995) 57–95.
[34] J. Antosiewicz, Computation of the dipole moments of proteins, Biophys. J. 69 (1995) 1344–1354.
[35] F.M. Richards, Areas, volumes, packing and protein structure, Ann. Rev. Biophys. Bioeng. 6 (1977) 151–176.
[36] M.K. Gilson, K.A. Sharp, B.H. Honig, Calculating the electrostatic potential of molecules in solution: Method and error assessment, J. Comput. Chem. 9 (1988) 327–335.
[37] M.E. Davis, J.A. McCammon, Calculating electrostatic forces from grid-calculated potentials, J. Comp. Chem. 11 (1990) 401–409.
[38] I. Klapper, R. Hagstrom, R. Fine, K. Sharp, B. Honig, Focusing of electric fields in the active site of Cu,Zn superoxide dismutase, Proteins: Struct. Func. Gen. 1 (1986) 47–79.
[39] D. Sitkoff, K.A. Sharp, B. Honig, Accurate calculation of hydration free energies using macroscopic solvent models, J. Phys. Chem. 98 (1994) 1978–1988.
[40] B.L. Kormos, Y. Benitex, A.M. Baranger, D.L. Beveridge, Affinity and specificity of protein U1A-RNA complex formation based on an additive component free energy model, J. Mol. Biol. 371 (2007) 1405–1419.
[41] J.M. Sturtevant, Heat capacity and entropy changes in processes involving proteins, Prot. Natl. Acad. Sci. U. S. A. 74 (1997) 2236–2240.
[42] A.V. Finkelstein, J. Janin, The price of lost freedom: entropy of bimolecular complex formation, Protein Eng. 3 (1989) 1–3.
[43] T. Lazaridis, A. Masunov, F. Gandolfo, Contributions to the binding free energy of ligands to avidin and streptavidin, Proteins 47 (2002) 194–208.
[44] S.D. Pickett, M.J.E. Sternberg, Empirical scale of side-chain conformational entropy in protein folding, J. Mol. Biol. 231 (1993) 825–839.
[45] D.D.L. Minh, J.M. Bui, C. Chang, T. Jain, J.M.J. Swanson, J.A. McCammon, The entropic cost of protein–protein association: a case study on acetylcholinesterase binding to fasciculin-2, Biophys. J. 89 (2005) L25–L27.
[46] J. Hermans, L. Wang, Inclusion of loss of translational and rotational freedom in theoretical estimates of free energies of binding: application to a complex of benzene and mutant T4 lysozyme, J. Amer. Chem. Soc. 119 (1997) 2707–2714.
[47] R. Luo, M.K. Gilson, Synthetic adenine receptors: direct calculation of binding affinity and entropy, J. Amer. Chem. Soc. 122 (2000) 2934–2937.
[48] J. Dziubiella, J.M.J. Swanson, J.A. McCammon, Coupling nonpolar and polar solvation free energies in implicit solvent models, J. Chem. Phys. 124 (2006) 084905.
[49] E. Gallicchio, R.M. Levy, AGBNP: An analytic implicit solvent model suitable for molecular dynamics simulations and high-resolution modeling, J. Comput. Chem. 25 (2004) 479–499.
[50] J.A. Wagoner, N.A. Baker, Assessing implicit models for nonpolar mean solvation forces: The importance of dispersion and volume terms, Proc. Natl. Acad. Sci. U.S.A. 103 (2006) 8331–8336.
[51] C. Tan, Y.H. Tan, R. Luo, Implicit nonpolar solvent models, J. Phys. Chem. B 111 (2007) 12263–12274.
[52] Z. Pilat, J.M. Antosiewicz, Multiple protonation equilibria in electrostatics of protein–protein binding, J. Phys. Chem. B 112 (2008) 15074–15085.